Interdisciplinary Sciences: Computational Life Sciences
https://doi.org/10.1007/s12539-018-0306-3

ORIGINAL RESEARCH ARTICLE

Computational Study of HCV p7 Channel: Insight into a New Strategy for HCV Inhibitor Design

Beili Ying[1,2] · Shichao Pang[3] · Junchen Yang[4] · Yang Zhong[1] · Jingfang Wang[5]

Received: 7 May 2018 / Revised: 23 July 2018 / Accepted: 3 September 2018

Abstract
HCV p7 protein is a cation-selective ion channel, playing an essential role during the life cycle of HCV viruses. To understand the cation-selective mechanism, we constructed a hexameric model in lipid bilayers of HCV p7 protein for HCB JFH-1 strain, genotype 2a. In this structural model, His9 and Val6 were key factors for the HCV cation-selective ion channel. The histidine residues at position 9 in the hexameric model formed a first gate for HCV p7 channel, acting as a selectivity filter for cations. The valines mentioned above formed a second gate for HCV p7 channel, serving as a hydrophobic filter for the dehydrated cations. The binding pocket for the channel blockers, e.g., amantadine and rimantadine, was composed of residues 20–26 in H2 helix and 52–60 in H3 helix in $i+2$ monomer. However, the molecular volumes for both amantadine and rimantadine were too small for the binding pocket of HCV p7 channel. Thus, designing a compound similar with rimantadine and having much larger volume would be an effective strategy for discovering inhibitors against HCV p7 channel. To achieve this point, we used rimantadine as a structural template to search ChEMBL database for the candidates employing favorable binding affinities to HCV p7 channel. As a result, six candidates were identified to have potential to be novel inhibitors against HCV p7 channel.

Keywords Hepatitis C virus · P7 channel · Structure-based drug design · Molecular modeling

1 Introduction

Hepatitis C is an infectious disease only found in humans and chimpanzees [1]. As estimated, approximately 150–200 million individuals worldwide are chronically infected with hepatitis C, causing 350,000 deaths every year due to the hepatitis C-related liver diseases [2, 3]. Thus, hepatitis C has been a global public health problem. The major problem for HCV treatment is lack of an effective vaccine or approved therapy specifically targeting on the HCV virus, which is regarded as the major reason for hepatitis C. Hepatitis C virus is a small enveloped, positive-sense single-strand RNA virus belonging to Flaviviridae family [4]. Many HCV direct-acting antiviral agents have been designed against hepatitis C virus, primarily targeting on only three virally non-structural proteins (NS3/4A protease; NS5A and NS5B RNA-dependent RNA polymerases) [5–8]. These proteins are essential during the RNA replication in the HCV viral life cycle. Currently, the standard of care treatment for HCV is the combinational use of pegylated interferon-alpha (IFN-α) and oral antiviral ribavirin [9]. With growing resistance to the current HCV direct-acting antiviral agents, we need to develop new drugs, not only targeting on the non-structural proteins, but also on the new virus proteins.

The entire HCV viral life cycle contains several major stages, including endocytosis and fusion, polyprotein synthesis from RNA and cleavage into individual proteins, RNA replication, as well as viral packaging and maturation. During this HIC viral life cycle, there are some

✉ Jingfang Wang
jfwang8113@sjtu.edu.cn

1 School of Life Sciences, Fudan University, Shanghai 200433, China

2 Shanghai Center for Bioinformation Technology, 1278 Keyuan Road, Shanghai 201203, China

3 Department of Statistics, School of Mathematical Sciences, Shanghai Jiao Tong University, Shanghai 200240, China

4 Department of Bioinformatics and Biostatistics, College of Life Science and Biotechnology, Shanghai Jiao Tong University, Shanghai 200240, China

5 Key Laboratory of Systems Biomedicine (Ministry of Education), Shanghai Center for Systems Biomedicine, Shanghai Jiao Tong University, Shanghai 200240, China

Published online: 07 September 2018

additional potential points for intervention, and a new strategy for developing HCV direct-acting antiviral agents is proposed by targeting on these points. Here, we focused on HCV p7 protein, a cation-selective ion channel [10]. This protein in the HCV viruses acts as an oligomeric proton channel to reduce the surrounding pH gradients in secretory vesicles, protecting the acid-labile intracellular virion during egress [11–13]. In the current study, we first constructed a three-dimensional structural model of HCV p7 protein in lipid bilayers based on the NMR studies [14]. Based on this computational model, we subsequently employed structure-based drug design and virtual screening to design novel inhibitors (or channel blockers) against HCV p7 channel.

2 Materials and Computational Methods

2.1 Constructing Structural Model for HCV p7 Channel

HCV p7 protein (JFH-1 strain, genotype 2a) with an accession number of Q99IB8 was selected as an original target. The solution NMR structure of HCV p7 protein from genotype 5a (PDB code: 2m6x) released in 2013 was selected as a template structure [14]. This NMR structure was the only structure showing a hexameric assembly in the RCSB Protein Data Bank (PDB). The initial structure of target p7 protein was constructed using Swiss-Model server [15]. Except for the polar hydrogen and heavy atoms in the initial structure, all the other atoms were removed. The p*K*a value for each residue was calculated by Delphi [16] with a dielectric constant of 4.0. Hydrogen atoms were subsequently added based on the computational p*K*a values mentioned above. The initial structure was then inserted into POPC lipid bilayers, and solvated in a simulation box ($110 \times 110 \times 90$ Å^3) with explicit TIP3P water molecules.

2.2 Generating p7-Rimantadine-Binding Model

Based on the computational models mentioned above, Q-SiteFinder [17] was employed to find the favorable ligand-binding site in HCV p7 protein. Rimantadine was then docked into the predicted binding site using AutoDock Vina [18]. The genetic algorithm was adopted to generate 10,000 independent runs on a 60-cubic-angstrom grid, centered on rimantadine with a grid spacing of 0.375 Å. The docking results for each independent run were clustered into several groups, and the binding model with lowest binding energy and favorable binding orientation was finally selected as the rimantadine-binding model for further analyses.

2.3 Molecular Dynamics Simulation

All the computational models were subjected to steepest descent energy minimization for about 5000 steps, followed by conjugate gradient for the next 5000 steps. Subsequently, all the models were equilibrated by a short molecular dynamics simulation (about 1 ns) with the heavy atoms of p7 protein, ligand, and lipid bilayers fixed. Finally, 20-ns molecular dynamics simulations were performed by AMBER 10 package [19] with periodic boundary condition and NPT ensemble. Temperature and pressure were maintained at 310 K and 1 bar using Langevin dynamics with a friction coefficient of 1.0 per ps and the Langevin piston method. SHAKE algorithm was used to constrain all bonds in the simulation systems, and atom velocities for start-up runs were obtained according to the Maxwell distribution at 310 K. For each simulation, at least three trajectories were generated with different starting atom velocities. The long-range electrostatic interactions were treated by the particle mesh Ewald (PME) method, with a grid point density of ~ 1 per cubic angstrom. The van der Waals interactions were calculated using a cutoff of 12 Å. All the molecular dynamics simulations were performed with a time step of 2 fs, and coordinates for all the models were saved every 1 ps.

2.4 Estimating Binding Free Energy for Rimantadine

The favorable binding models for rimantadine were subjected to a short molecular dynamics simulation (~ 1 ns) using the parameters and setting mentioned above. The molecular mechanics Poisson–Boltzmann surface area (MM-PB/SA) approach was subsequently used to estimate the binding free energy for rimantadine in the favorable binding models. In the MM-PB/SA approach, the binding free energy for rimantadine was calculated as the difference value between the free energies of p7–rimantadine complex, p7 channel, and rimantadine. These free energies were estimated as the sum of the internal energy in the gas and solvation-free energy. The former was treated as a standard force field energy calculated by the strain energy from covalent, torsion angle, non-covalent van der Waals, and electrostatic energy. The latter was calculated based on an electrostatic term and a non-polar component. The electrostatic term was computed by the Poisson–Boltzmann equation, while the non-polar component was estimated by the molecular solvent surface area (SASA).

2.5 Virtual Screening Procedure for New Inhibitors Against p7 Channel

Rimantadine was selected as a structural template to search the bioactive drug-like small molecules in ChEMBL

database. MACCS keys [20] were employed to find those molecules that had high similarity with the template rimantadine, which was further assessed by Lipinski's Rule Five. The candidates in accordance with Lipinski's Rule Five were subsequently subject to docking procedures using AutoDock Vina. Finally, the candidates with similar or higher binding energies than the template rimantadine were selected.

3 Results and Discussion

3.1 Structural Model of HCV p7 Protein

HCV p7 protein monomer is a 63-residue transmembrane protein including an N-terminal helix H1 (residues 5–16), a middle helical part H2 (residue 20–41), and a C-terminal helix H3 (residues 48–58) [21, 22]. This protein oligomerizes to form an ion channel with specific cation selectivity (usually for calcium ions over potassium and sodium ions) [10, 23]. Nuclear magnetic resonance study showed that the p7 hexamer was flower-like shape, in which one monomer (*i*) can not only interact with neighboring one, but also contact with $i+2$ and $i+3$ monomers (Fig. 1) [14]. In this form, H1 and H2 helices are the essential components for the channel interior with the lipid-facing H3 helix packing against H1 helix of the $i+3$ monomer and H2 helix of the $i+2$ monomer.

In the structural model of HCV p7 channel, the histidine and valine residues at position 9 and 6, respectively, were identified as key residues to regulate the gate opening for the HCV p7 hexamer channel (Fig. 2a). The histidine residues at position 9 formed the narrowest conical region of the channel with a pore radius of ~ 1.27 Å (Fig. 2b). These histidine residues were regarded to be the first gate of HCV p7 channel with affinity for both monovalent and divalent cations, e.g., calcium, potassium, and sodium ions, as they acted as a selectivity filter to dehydrate monovalent and divalent cations. Additional experiments showed that the substitution of alanine for histidine at this position would induce a nearly 70% reduction in the channel conductance [14]. The second gate of HCV p7 channel was formed by Val6 with a pore radius of nearly 2.39 Å (Fig. 2b). This valine residue served as a hydrophobic filter to allow the dehydrated cations going through the channel.

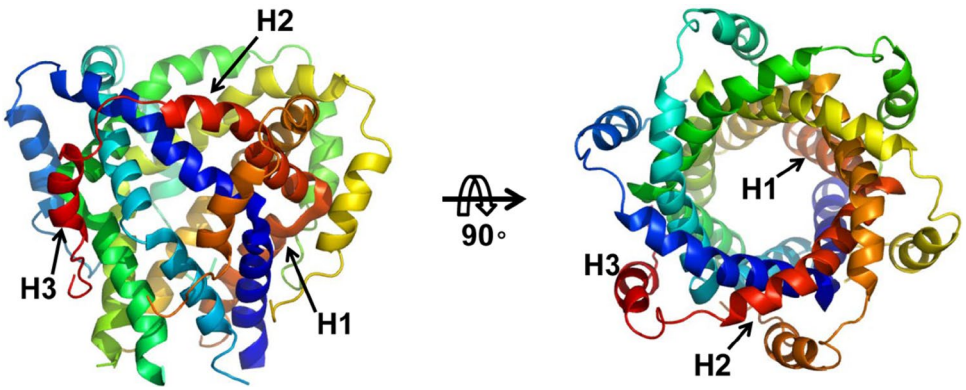

Fig. 1 Structural model of HCV p7 protein. HCV p7 protein showed a flower-like hexameric assembly, oligomerizing an ion-selective channel. Each p7 monomer contains 63 residues, constituted of an N-terminal helix H1 (residues 5–16), a middle helical part H2 (residue 20–41), and a C-terminal helix H3 (residues 48–58)

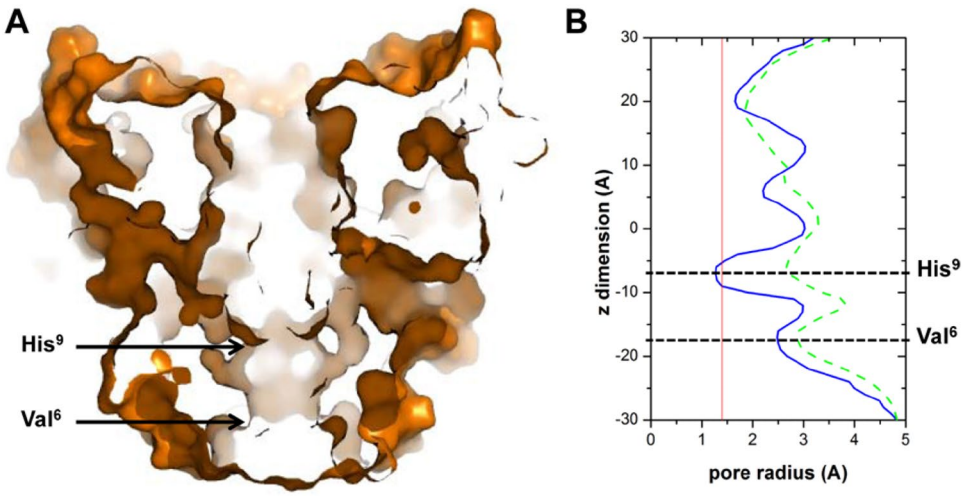

Fig. 2 Channel pore of HCV p7 protein. His9 and Val6 were key residues for HCV p7 channel. **a** Perspective view of the channel pore. His9 formed the first gate of p7 hexamer channel, acting as a selectivity filter for cations. Val6 was the second gate, serving as a hydrophobic filter for the dehydrated cations. **b** Radial profile of the pore for open (green dotted line) and closed (blue solid line) p7 channels

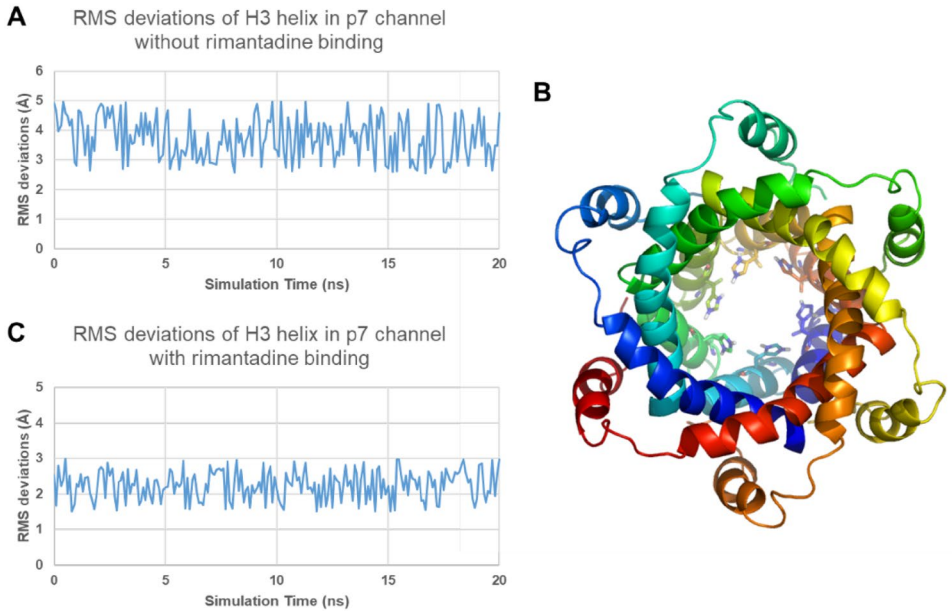

Fig. 3 Flexibility of H3 helix. **a** RMS deviations of H3 helix in HCV p7 channel in the apo form. **b** Open state of HCV p7 channel. In this state, the narrowest channel pore of p7 channel formed by histidine residues was nearly 2.7 Å. **c** RMS deviations of H3 helix in HCV p7 channel with rimantadine binding

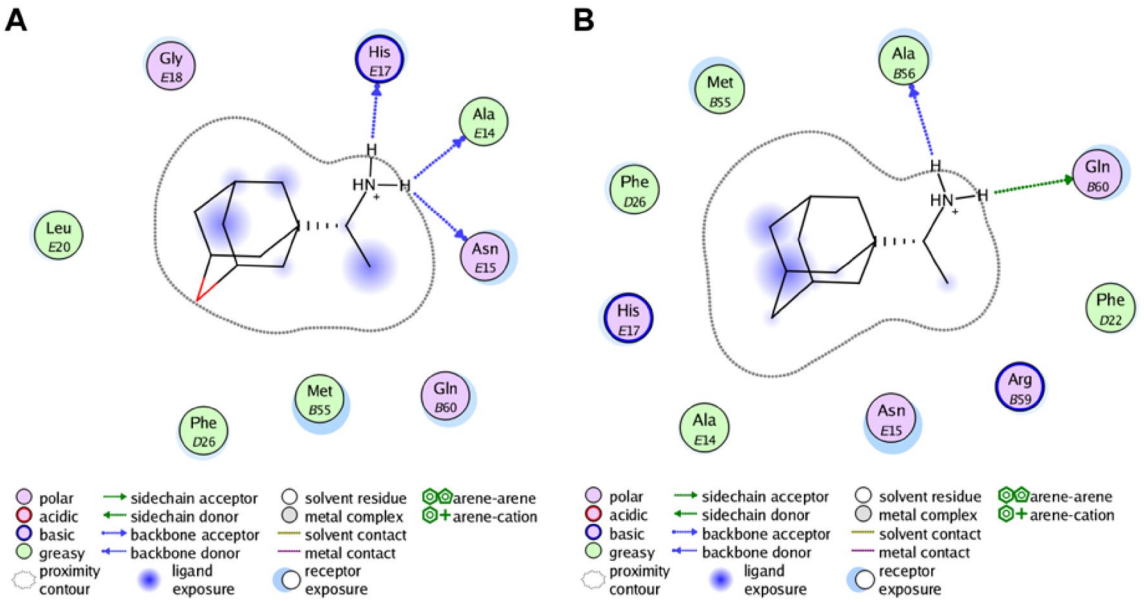

Fig. 4 Possible binding models of rimantadine. **a** Rimantadine-binding model (I) Ala14, Asn15, and His17 functioned to recognize and position the substrate by multiple hydrogen-bonding interactions (blue dotted arrows). While residues 55–60 in $i+2$ monomer provided the hydrophobic interactions for substrate binding. **b** Rimantadine-binding model (II) Ala56 and Gln60 formed hydrogen bonds with the substrate, while residues 22–26 in $i+1$ monomer and 14–17 in $i+2$ monomer exhibited hydrophobic contacts with the substrate

3.2 Rimantadine Binding and Inhibition Mechanism

As shown in Fig. 2, the structural model of HCV p7 protein was in a closed state, in which the narrowest channel pore was only 1.27 Å, smaller than the van der Waals radius of water molecules (~ 1.4 Å). However, H3 helix showed a significant flexibility during our simulations (Fig. 3a). Due to the flexibility of H3 helix, p7 channel would adopt an open state (Fig. 3b), in which the narrowest channel pore became 2.7 Å. In the open state, water molecules were able to go through the first gate formed by histidine rings. Therefore, to reduce the channel activity, we need to inhibit the movement of H3 helix. Adamantane and rimantadine were well-known channel blockers, whose derivatives were used in HCV clinical trials [24, 25]. We finally docked rimantadine

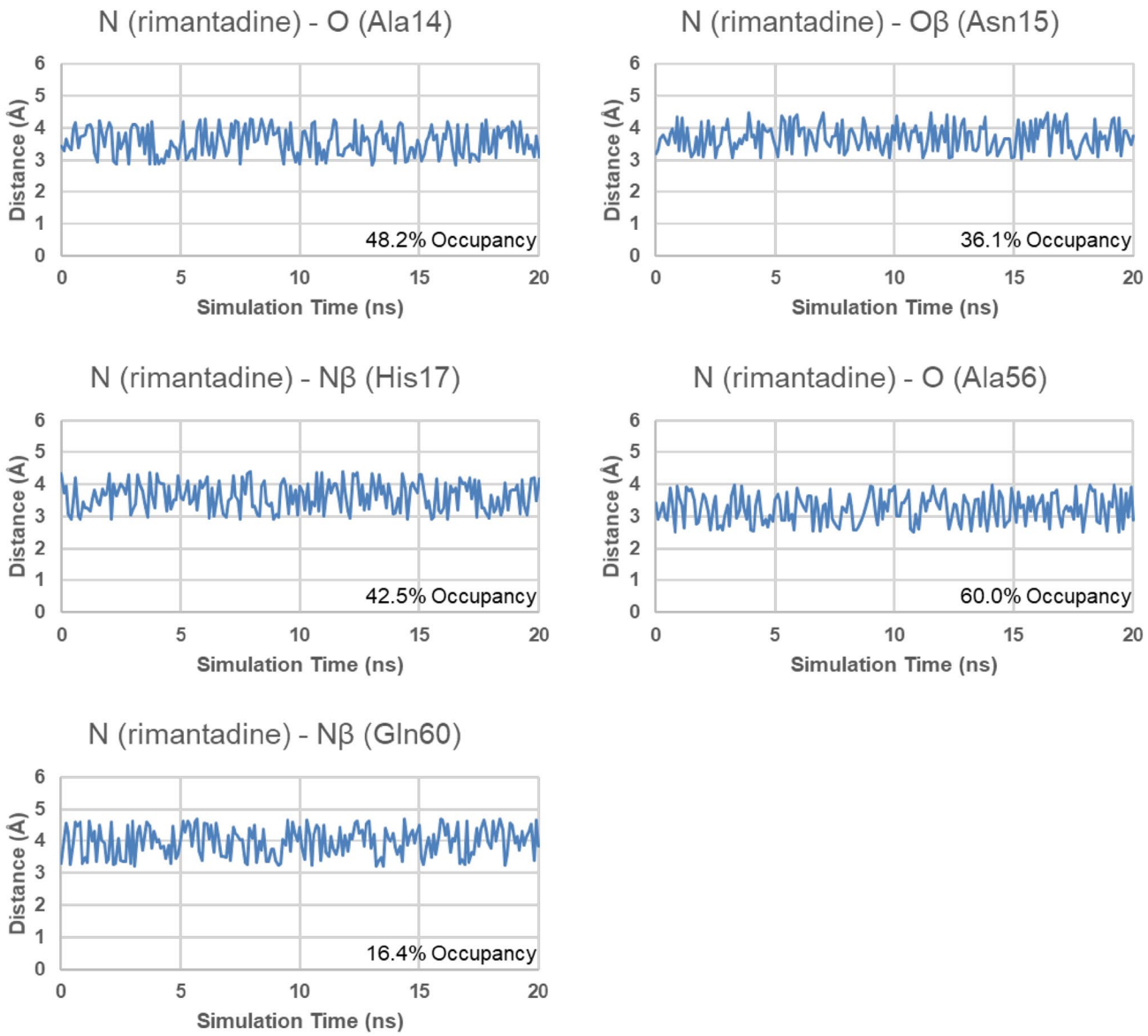

Fig. 5 Heavy atom distances of hydrogen donors and receptors. In the first binding model, Ala14, Asn15, and His17 formed hydrogen bonds with the amino group of rimantadine with occupancies of 48.2%, 36.1%, and 42.5%, respectively. In the second binding model, Ala56 and Gln60 formed hydrogen bonds with the amino group of rimantadine with occupancies of 60.0% and 16.4%, respectively

into the binding pocket identified by Q-SiteFinder, and got two possible binding models (Fig. 4).

Generally speaking, rimantadine was docked into the same pocket in both selected binding models. Therefore, the estimated binding free energies for the two possible binding models were identical (− 6.95 kcal/mol calculated by MM-PB/SA approach). Structural analysis indicated that hydrogen-bonding and hydrophobic interactions made a significant contribution to binding free energy of rimantadine. In the current study, if the heavy atoms of the hydrogen donor and the acceptor were less than 3.5 Å, they were considered to form a hydrogen bond; if the mass center of two hydrophobic surfaces was less than 6.5 Å, they were considered to form a hydrophobic interaction.

In the first binding model (Fig. 4a), Ala14, Asn15, and His17 were key residues for rimantadine binding. These residues formed significant hydrogen bonds with the amino group of rimantadine. As shown in Fig. 5, distance monitoring indicated that the occupancies of the hydrogen bonds formed by the residues mentioned above were 48.2%, 36.1%, and 42.5%, respectively. These hydrogen bonds functioned to recognize and position rimantadine in a favorable orientation. Residues 55–60 in $i+2$ monomer provided hydrophobic interactions with rimantadine to enhance the binding

affinity. The occupancy of the hydrophobic interactions formed by the aforementioned residues was 35.8% (Fig. 6).

In the second binding model (Fig. 4b), rimantadine was fixed by Ala56 and Gln60 in the binding pocket via hydrogen-bonding interactions. The occupancies of the hydrogen bonds formed by Ala56 and Gln60 were 60.0% and 16.4%, respectively (Fig. 5), giving an indication that Ala56 was the essential residue for the binding of rimantadine. Similar with the first binding model, residues 22–26 in $i+1$ monomer and 14–17 in $i+2$ monomer played important roles for providing hydrophobic interactions with rimantadine. The occupancy of the hydrophobic interactions formed by the aforementioned residues was 24.4% (Fig. 6).

In both binding models, rimantadine was positioned in the same binding pocket (residues 20–26 in H2 helix and 52–60 in H3 helix in $i+2$ monomer), which was further confirmed by solution NMR and mutagenesis studies [14, 25–27]. Drugs binding in the pocket mentioned above would enhance the connects between H2 and H3 helices and fix H3 helix in a position close to H2 helix in $i+2$ monomer. Compared with the apo form of p7 channel, H3 helix showed a significant reducement in RMS deviation values after rimantadine binding (Fig. 3c). However, the open state of HCV p7 channel needs the structural rearrangement in the intervening loop between H2 and H3 helices. By binding to the key position, rimantadine could set H2 and H3 helices in stabilized positions, further reducing the probability of opening the channel.

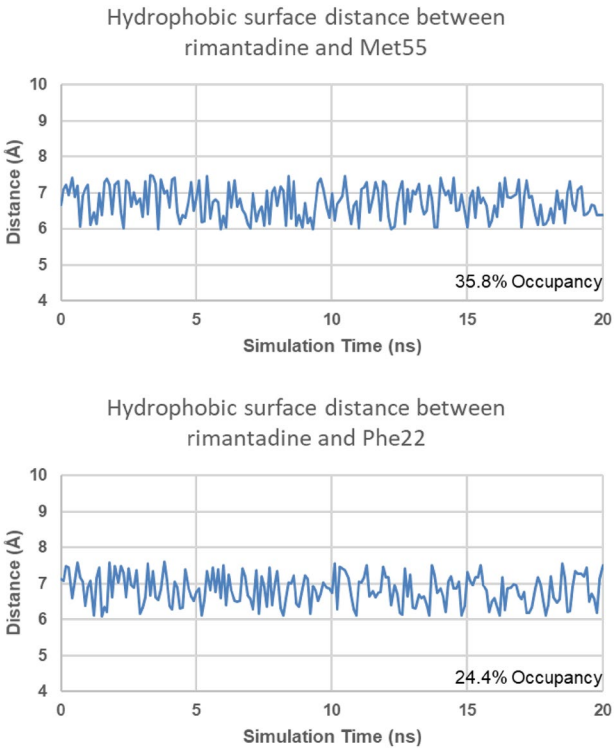

Fig. 6 Hydrophobic surface distance between rimantadine and residues in the binding site. In the first binding model, the hydrophobic interactions were found between rimantadine and hydrophobic surface centered on Met55 with an occupancy of 35.8%. In the second binding model, the hydrophobic interactions were found between rimantadine and hydrophobic surface centered on Phe22 with an occupancy of 24.4%

3.3 Structure-Based Inhibitor Design

Based on the structural and computational analyses mentioned above, we could obtain a deep insight into the drug-binding models for HCV p7 channel. Based on this knowledge, we could design novel inhibitors against HCV p7 channel. In the current case, rimantadine was too small and could not entirely occupy identified binding pocket (Fig. 7). Thus, we could design some compounds that employed larger size than rimantadine and could entirely occupy the identified binding pocket. We used rimantadine as a structural template to search ChEMBL database, and finally, six candidates were identified (Fig. 7).

To check the druggabilities of the identified candidates, we also made ADME predictions (Table 1). According to the Lipinski's Rule of Five, the orally active drugs should have no more than one violation of the following criteria: (i) no more than five hydrogen-bond donors and ten hydrogen-bond acceptors, (ii) molecular mass less than 500 Da, and (iii) the octanol–water partition coefficient log$P$ in -0.4 to 5.6 range. All the criteria for the identified candidates were within the acceptable ranges of the Lipinski's Rule of Five, indicating that these compounds reported in the current study could be used as potential leading compounds for further drug design against HCV p7 protein.

4 Conclusion

In the current study, we constructed a three-dimensional structural model of HCV p7 protein in lipid bilayers. The hexamer of this protein exhibited a cation-selective ion channel with flower-like shape. Based on the structural analysis, His9 and Val6 were regarded as gating residues for HCV p7 channel, forming the narrowest parts of the channel pore. The famous channel blocker, rimantadine, was found to bind in the pocket formed by residues 20–26 in H2 helix and 52–60 in H3 helix in $i+2$ monomer. However, due to the small size, rimantadine could not entirely occupy the binding pocket. We used rimantadine as a structural template to search ChEMBL database, and found six candidates that had higher binding affinities than rimantadine and comparatively lower toxicities in human body. We believed that these

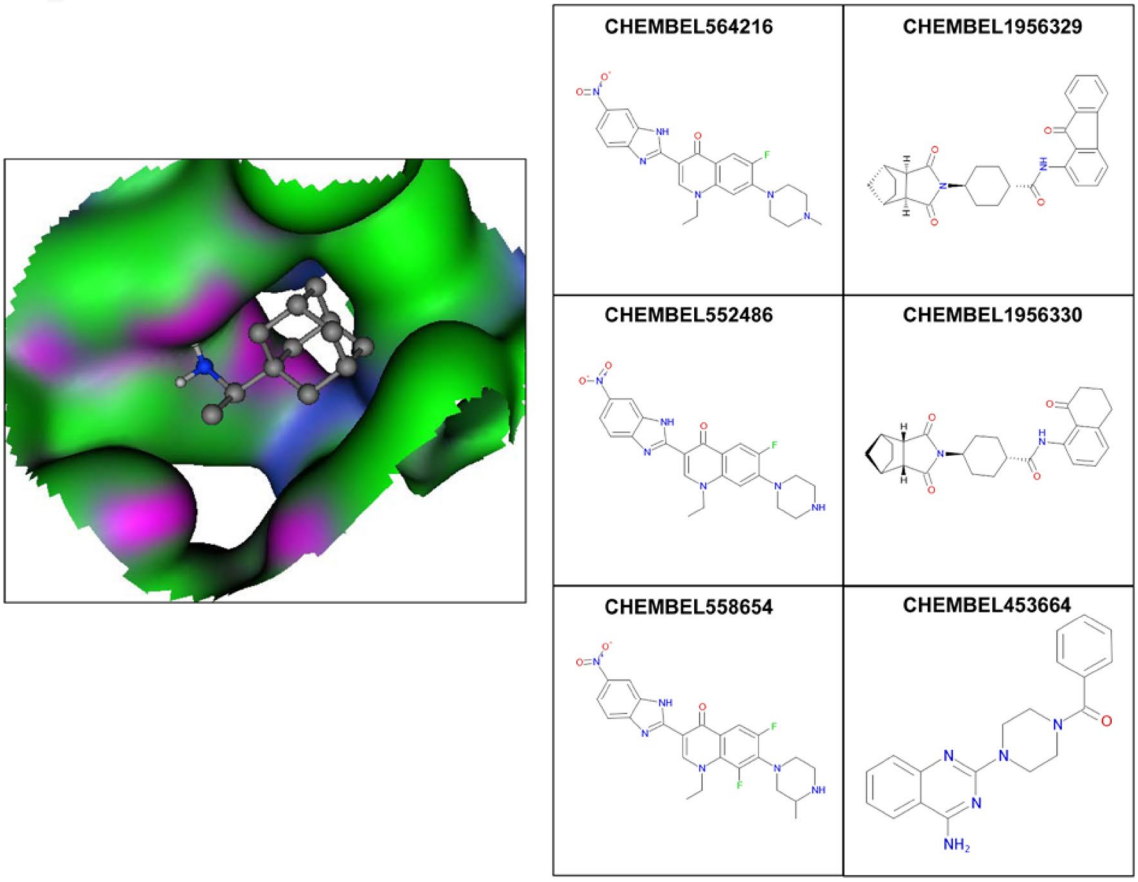

Fig. 7 Binding pocket of rimantadine in HCV p7 protein. Left panels: the hydrophobic and hydrophilic surfaces were colored in green and blue; the surface for hydrogen-binding interactions was in pink. Right panels: final candidates obtained from ChEMBL database using rimantadine as a structural template

Table 1 MADE properties of the final candidates obtained from ChEMBL database

No.	ID	Mol_MW[a]	H don[b]	H acc[c]	*Alog*P[d]	PSA[e]	*Alog*S[f]
1	564,216	450.47	1	7	3.54	101.29	−3.66
2	552,486	436.44	2	7	3.00	110.07	−3.87
3	558,654	468.46	2	7	3.58	110.07	−4.07
4	1,956,329	434.53	1	4	3.27	83.55	−4.22
5	1,956,330	468.54	1	4	3.85	83.55	−4.89
6	453,664	333.39	1	5	2.75	75.35	−3.04

[a]The molecular mass (Mol_MW) should be less than 500 Da

[b]The hydrogen-bond donors (H donor) should be no more than five

[c]The hydrogen-bond acceptors (H acceptor) should be no more than ten

[d]The predicted octanol/water partition coefficient (−0.4 to 5.6)

[e]The van der Waals surface area of polar nitrogen and oxygen atoms (7.0–200)

[f]The predicted aqueous solubility *S* (mol dm^{-3}) is the concentration of the solute in a saturated solution that is in equilibrium with the crystalline solid (−6.5 to 0.5)

reported compounds could be used as potential leading compounds for further inhibitor design against HCV p7 protein, providing a novel strategy for HCV treatment.

Acknowledgements This work was supported by the National Key Research and Development Program of China (no. 2016YFA0500600).

References

1. Mohd Hanafiah K, Groeger J, Flaxman AD, Wiersma ST (2013) Global epidemiology of hepatitis C virus infection: new estimates of age-specific antibody to HCV seroprevalence. Hepatology 57(4):1333–1342
2. Shepard CW, Finelli L, Alter MJ (2005) Global epidemiology of hepatitis C virus infection. Lancet Infect Dis 5(9):558–567
3. Lauer GM, Walker BD (2001) Hepatitis C virus infection. N Engl J Med 345(1):41–52
4. Seeff LB (1997) Natural history of hepatitis C. Hepatology 26 (3 Suppl 1):21S-28S
5. de Vicente J, Hendricks RT, Smith DB, Fell JB, Fischer J, Spencer SR, Stengel PJ, Mohr P, Robinson JE, Blake JF, Hilgenkamp RK, Yee C, Adjabeng G, Elworthy TR, Tracy J, Chin E, Li J, Wang B, Bamberg JT, Stephenson R, Oshiro C, Harris SF, Ghate M, Leveque V, Najera I, Le Pogam S, Rajyaguru S, Ao-Ieong G, Alexandrova L, Larrabee S, Brandl M, Briggs A, Sukhtankar S, Farrell R, Xu B (2009) Non-nucleoside inhibitors of HCV polymerase NS5B. Part 2: Synthesis and structure-activity relationships of benzothiazine-substituted quinolinediones. Bioorg Med Chem Lett 19(13):3642–3646
6. Gao M, Nettles RE, Belema M, Snyder LB, Nguyen VN, Fridell RA, Serrano-Wu MH, Langley DR, Sun JH, O'Boyle DR 2nd, Lemm JA, Wang C, Knipe JO, Chien C, Colonno RJ, Grasela DM, Meanwell NA, Hamann LG (2010) Chemical genetics strategy identifies an HCV NS5A inhibitor with a potent clinical effect. Nature 465(7294):96–100
7. Legrand-Abravanel F, Nicot F, Izopet J (2010) New NS5B polymerase inhibitors for hepatitis C. Expert Opin Investig Drugs 19(8):963–975
8. Sofia MJ, Chang W, Furman PA, Mosley RT, Ross BS (2012) Nucleoside, nucleotide, and non-nucleoside inhibitors of hepatitis C virus NS5B RNA-dependent RNA-polymerase. J Med Chem 55(6):2481–2531
9. Zeuzem S (2008) Interferon-based therapy for chronic hepatitis C: current and future perspectives. Nat Clin Pract Gastroenterol Hepatol 5(11):610–622
10. Pavlovic D, Neville DC, Argaud O, Blumberg B, Dwek RA, Fischer WB, Zitzmann N (2003) The hepatitis C virus p7 protein forms an ion channel that is inhibited by long-alkyl-chain iminosugar derivatives. Proc Natl Acad Sci USA 100(10):6104–6108
11. Jones CT, Murray CL, Eastman DK, Tassello J, Rice CM (2007) Hepatitis C virus p7 and NS2 proteins are essential for production of infectious virus. J Virol 81(16):8374–8383
12. Steinmann E, Penin F, Kallis S, Patel AH, Bartenschlager R, Pietschmann T (2007) Hepatitis C virus p7 protein is crucial for assembly and release of infectious virions. PLoS Pathog 3(7):e103
13. Wozniak AL, Griffin S, Rowlands D, Harris M, Yi M, Lemon SM, Weinman SA (2010) Intracellular proton conductance of the hepatitis C virus p7 protein and its contribution to infectious virus production. PLoS Pathog 6(9):e1001087
14. OuYang B, Xie S, Berardi MJ, Zhao X, Dev J, Yu W, Sun B, Chou JJ (2013) Unusual architecture of the p7 channel from hepatitis C virus. Nature 498(7455):521–525
15. Arnold K, Bordoli L, Kopp J, Schwede T (2006) The SWISS-MODEL workspace: a web-based environment for protein structure homology modelling. Bioinformatics 22(2):195–201
16. Georgescu RE, Alexov EG, Gunner MR (2002) Combining conformational flexibility and continuum electrostatics for calculating p*K*(a)s in proteins. Biophys J 83(4):1731–1748
17. Laurie AT, Jackson RM (2005) Q-SiteFinder: an energy-based method for the prediction of protein-ligand binding sites. Bioinformatics 21(9):1908–1916
18. Trott O, Olson AJ (2010) AutoDock Vina: improving the speed and accuracy of docking with a new scoring function, efficient optimization, and multithreading. J Comput Chem 31(2):455–461
19. Case DA, Cheatham TE 3rd, Darden T, Gohlke H, Luo R, Merz Jr KM, Onufriev A, Simmerling C, Wang B, Woods RJ (2005) The Amber biomolecular simulation programs. J Comput Chem 26(16):1668–1688
20. Thorner DA, Willett P, Wright PM, Taylor R (1997) Similarity searching in files of three-dimensional chemical structures: representation and searching of molecular electrostatic potentials using field-graphs. J Comput Aided Mol Des 11(2):163–174
21. Montserret R, Saint N, Vanbelle C, Salvay AG, Simorre JP, Ebel C, Sapay N, Renisio JG, Bockmann A, Steinmann E, Pietschmann T, Dubuisson J, Chipot C, Penin F (2010) NMR structure and ion channel activity of the p7 protein from hepatitis C virus. J Biol Chem 285(41):31446–31461
22. Cook GA, Opella SJ (2011) Secondary structure, dynamics, and architecture of the p7 membrane protein from hepatitis C virus by NMR spectroscopy. Biochim Biophys Acta 1808(6):1448–1453
23. Premkumar A, Wilson L, Ewart GD, Gage PW (2004) Cation-selective ion channels formed by p7 of hepatitis C virus are blocked by hexamethylene amiloride. FEBS Lett 557(1–3):99–103
24. Griffin SD, Beales LP, Clarke DS, Worsfold O, Evans SD, Jaeger J, Harris MP, Rowlands DJ (2003) The p7 protein of hepatitis C virus forms an ion channel that is blocked by the antiviral drug, amantadine. FEBS Lett 535(1–3):34–38
25. Mihm U, Grigorian N, Welsch C, Herrmann E, Kronenberger B, Teuber G, von Wagner M, Hofmann WP, Albrecht M, Lengauer T, Zeuzem S, Sarrazin C (2006) Amino acid variations in hepatitis C virus p7 and sensitivity to antiviral combination therapy with amantadine in chronic hepatitis C. Antivir Ther 11(4):507–519
26. Foster TL, Verow M, Wozniak AL, Bentham MJ, Thompson J, Atkins E, Weinman SA, Fishwick C, Foster R, Harris M, Griffin S (2011) Resistance mutations define specific antiviral effects for inhibitors of the hepatitis C virus p7 ion channel. Hepatology 54(1):79–90
27. Castelain S, Bonte D, Penin F, Francois C, Capron D, Dedeurwaerder S, Zawadzki P, Morel V, Wychowski C, Duverlie G (2007) Hepatitis C virus p7 membrane protein quasispecies variability in chronically infected patients treated with interferon and ribavirin, with or without amantadine. J Med Virol 79(2):144–154